WILEY-VCH

Monochromatic Blue and Switchable Blue-Green Carbon Quantum Dots by Room-temperature Air Plasma Processing

Janith Weerasinghe[#], James Scott[#], Athukoralalage Don K. Deshan, Dechao Chen, Amandeep Singh, Suvankar Sen, Prashant Sonar, Krasimir Vasilev, Qin Li, and Kostya (Ken) Ostrikov[*]*

J. Weerasinghe, Dr. A. Singh, Prof. P. Sonar, Prof. K. Ostrikov
School of Chemistry and Physics, Queensland University of Technology, Brisbane 4000, Australia
E-mail: kostya.ostrikov@qut.edu.au

J. Scott, Dr. D. Chen, Prof. Q. Li
Queensland Micro- and Nanotechnology Centre, School of Engineering and Built Environment, Griffith University, Nathan, Queensland 4111, Australia
E-mail: qin.li@griffith.edu.au

A.D.K. Deshan
Centre for Agriculture and the Bioeconomy, Queensland University of Technology, Brisbane 4000, Australia

S. Sen
School of Engineering, RMIT University, Melbourne, Victoria 3000, Australia

Prof. K. Vasilev
School of Engineering, University of South Australia, Adelaide 5001, South Australia, Australia

[#] equal contributions

Keywords: Carbon quantum dots, Atmospheric pressure plasma, Duel emissive carbon dots, Copper ion sensing

Carbon quantum dots (CQDs, C-dots or CDs) are an emerging type of nanomaterial which has received immense attention due to their numerous applications. However, most of the reported CQDs in literature typically emit single emission peak under an excitation. Multipeak

emissions without any complicated techniques will be ideal for various applications in the fields of ratiometric sensing, optoelectronics, and multifunctional bio imaging systems. Here, fast, effective, and a single step method was developed for the bulk synthesis of CQDs using atmospheric pressure air plasmas. Structural, morphological, and chemical properties were characterised by advanced analytical techniques. The CQDs have the average diameter of about 3 nm with a narrow size distribution. Emission wavelengths of 470 nm for blue emissive CQDs and 515 nm for green emissive CQDs were observed. Concentration dependency of the CQDs suggests that the switchable mechanism is due to the formation of PTSA excimers. Dual-emissive CQDs have potential to be used in bi-channel ratiometric determination for metal ions, pH sensing, tumour diagnosis and detection, and solid-state lighting materials. The proof-of-principle demonstration of the use of dual-emissive CQDs (DCQDs) as a fluorescent sensor of Cu^{2+} ions was also presented to highlight the possible applications.

1. Introduction

The diverse family of nanomaterials can be derived from carbon such as graphene, fullerenes, nanotubes, nanofibers, nanodiamonds, and carbon quantum dots (CQDs).[1] CQDs feature properties such as high-water solubility, low toxicity, higher biocompatibility, low cost, and unique optical performance.[2] Various methods have been used for the synthesis of CQDs such as pyrolysis, carbonization, microwave irradiation, hydrothermal techniques, etc.[3] The mechanisms responsible for the fluorescence of the CQDs have been attributed to electronic bandgap transitions of conjugated π domains, surface defects, elemental doping and fluorophores.[4] Some of the above mechanisms take part in the dual emissive nature of CQDs. However, according to most of the published work, excitation dependent fluorescence of CQDs is caused by the energy gap traps of the surface localized states.[5]

Several synthetic pathways are available for synthesizing CQDs. The top-down methods using bulk carbon sources such as graphite, carbon fibres or carbon nanotubes and the bottom-up methods carbonize molecular precursors such as carbohydrate, organic compounds, or amino acids. Different techniques such as microwave, hydrothermal, pyrolysis, laser ablation, arc discharge, etc. can be used for this process. Hydrothermal is the most extensively used method for the CQD synthesis due to the simplicity of the setup and the reasonable uniformity of the synthesized CQDs.[1] However, limitations of this technique include the longer reaction time of several hours required to complete the reaction.[6] The arc discharge is another method adapted to synthesize CQDs. During the arc discharge, carbon atoms are removed from bulk carbon precursor via a gas plasma. Large particle size distribution can be found in the resulting CQDs which is the main drawback of this technique. The laser ablation technique uses a high-power laser beam to bombard the surface of a targeted precursor material which evaporates and recrystallizes it, forming nanoparticles. Unlike in arc discharge technique, CQDs synthesized by laser ablation have narrow size distribution. However, it is a complicated process, and the operating cost is not yet suitable for industrial applications.[7] Other synthetic routes for CQDs including microwave pyrolysis, chemical oxidation, and electrochemical methods which all have their pros and cons with regards to large-scale production. However, an efficient and scalable production method to produce CQDs for commercial application remains a limitation for all of the technologies mentioned.[2] Moreover, synthetic methods for dual-emissive CQDs are rarely reported. Most of these techniques involves complex preparation, modification, or conjugation procedures.[8] Here we report a low-temperature plasma-based method which helps resolve the above issues.

Plasma is one of the fundamental states of matter and a typical plasma contains charged species, photons, as well as atomic, molecular, and radical species. Cold plasmas can be generated without using expensive vacuum systems, pumps, or any other sophisticated instrument.

Energetic species in plasma can participate in a number of processes such as ionization, excitation, and dissociation, which can be typically initiated only in more extreme reaction conditions. Due to these unique advantages of the plasma technology, it can be used in a number of applications including plasma sintering, bacterial inactivation, water desalination, nanomaterial synthesis, surface modification and materials deposition.[9]

Few reports can be found which use cold atmospheric plasmas to produce CQDs featuring a single emission wavelength. Xu et al.[10] synthesized amorphous carbon supported Pt nanoparticle composite via a DC plasma reactor using Argon as the career gas. Chloroplatinic acid ($HPtCl_6$ $6H_2O$) was used at the platinum (Pt) precursor and ethanol (C_2H_5OH) was used as both solvent and carbon source.[10] Graphene quantum dot wrapped in gold nanoparticles were created by DC microplasma by Kumar et al.[11] Blue emissive CQDs have been synthesized using different carbon precursors such as sodium dodecyl sulfate[12], chitosan[13], hydrocarbons[14], citric acid[15], D-fructose[16], and folic acid.[17] CQDs synthesis was successfully performed under both acidic and basic reaction environments. N-doping of the CQDs was achieved by simply adding a nitrogen source to the precursor. For example, blue emissive CQDs have been synthesised by Ma et al. using a DC microplasma reactor with Ar gas.[18] They synthesized N-doped CQDs via the same experimental setup only by changing the precursor to a mixture of citric acid and ethylenediamine where ethylenediamine acted as a nitrogen dopant.[19]

The similarity in all these reports is the use of inert gas as the plasma carrier gas. Also, most of these syntheses were conducted using DC microplasma equipment. Dager et al. took a different approach using a microwave plasma with hydrogen gas for the conversion of fenugreek seeds directly into blue emissive CQDs.[20] They identified that the high energy electrons and excited hydrogen ions played a major role on the direct conversion of the precursor into CQDs. Reports

on plasma synthesised CQDs in wavelengths other than blue are rare. Interestingly, yellow emissive carbon dots were created by Qin et al. by Argon microplasma using O-phenylamine as the carbon precursor, which has been successfully employed in cell imaging experiments.[21]

Therefore, problem of synthesising dual-emissive CQDs via a simple and scalable technique remains as an urgent requirement for the development of the next-generation technologies. In this work, we have resolved this problem, for the first time, by employing atmospheric air to generate cold plasma for the blue and green/blue switchable CQDs synthesis (**Figure 1**). Also, such technique has not been reported previously according to the best of our knowledge. The produced CQDs are of diameter around 3 nm and exhibit emission peaks around 470 nm for blue colour and 515 nm for green colour. Ultraviolet and visible (UV-Vis) absorbance, Fourier transform infrared (FTIR), transmission electron microscopy (TEM), X-ray photoelectron spectroscopy (XPS), photoluminescence spectrometry (PL), Dynamic Light Scattering (DLS), Optical Emission Spectroscopy (OES), techniques are used to analyse the produced CQDs and determine the plasma chemical mechanisms taking place during the CQDs formation. CQDs can be produced within minutes in this single-step process at low temperatures under 100 ^{0}C. This work provides a simple, scalable, and environmentally friendly method to synthesize CQDs under ambient conditions which are favourable for commercial bulk production. The underlying mechanisms and potential applications of this unique feature are also discussed.

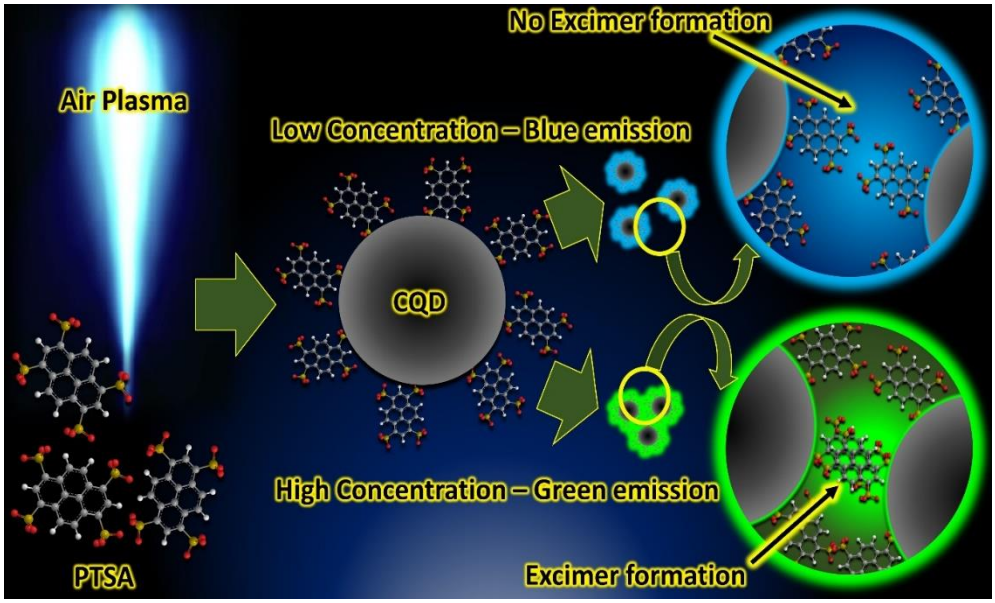

Figure 1: Synthesis and dual-emission mechanisms of CQDs by air plasma technique

2. Results and discussion

Blue/green switchable emissive carbon dots (DCQD) have been synthesized from 1,3,6,8-Pyrenetetrasulfonic acid tetrasodium salt hydrate (PTSA) using cold atmospheric plasma. DCQDs exhibit a narrow peak in the excitation spectra while blue emissive carbon dots (BCQD) synthesized from urea and citric acid, show a broad double peak (**Figure 2A**). The UV-vis absorption spectra of BCQDs possess a strong saturated peak at 240 nm which indicates π-π* transitions of C=C bond (**Figure 2B**). A weaker absorption peak in the range of 310 - 350 nm can be found from n-π* transitions of C=O/N.[22] Similarly, a weaker absorption peak can be seen for DCQD in the range of 440 - 510 nm.

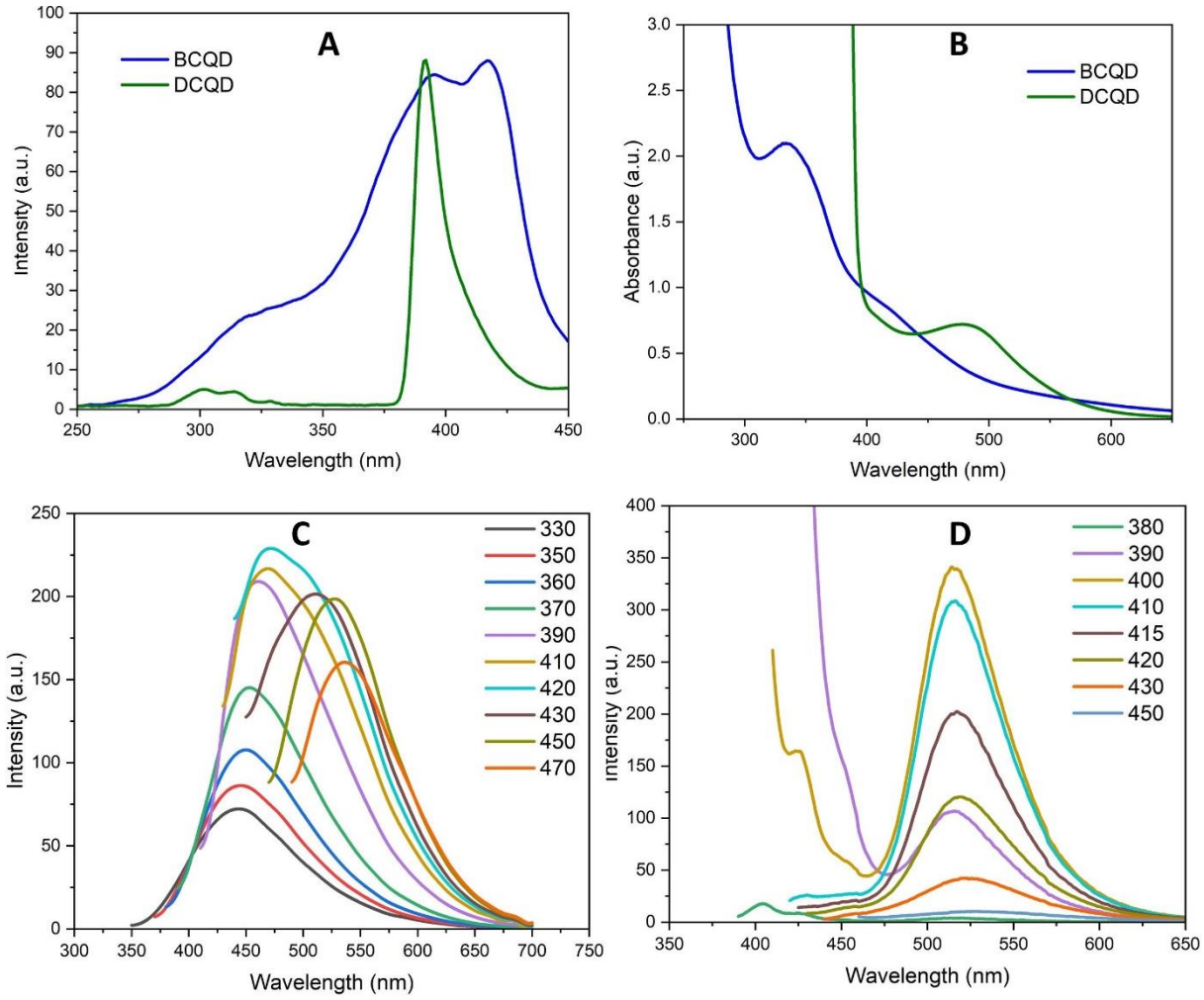

Figure 2: Emission properties of the blue emissive carbon dots (BCQDs) and blue/green switchable emissive carbon dots (DCQDs). A:PL excitation spectra, B: UV-Visible absorption spectra, C: PL emission spectra of BCQDs and D: PL emission spectra of DCQDs

The PL performance of the CQDs was investigated as shown in **Figure 2C** and **2D**. The luminescent mechanism for CQDs can be caused by either the band gap states of the conjugated domains or surface defects.[6] The maximum emission peak for BCQDs is centred at 470 nm under 420 nm excitation indicating the blue emission. Similarly, the maximum emission peak for DCQDs is peaked at 515 nm under the excitation of 400 nm (**Figure D**). Unlike BCQDs, the emission position of PL had not changed when the excitation wavelength was varied from 380 to 450 nm except the emission intensity.

The fluorescence of DCQDs is strongly concentration dependent, exhibiting a deep purple fluorescence at concentrations ≤1g/L with a QY of ~35%, and green emissions at concentrations ≥1g/L, both emissions are present at and around 1g/L. The purple fluorescence shown in **Figure 3B** and **Figure S7** is characteristic of a small polycyclic molecule, with a series of narrow peaks separated by ~160 meV (7.75μm) associated with the C-C stretching vibrations of polyaromatic hydrocarbons (6-8 μm).[23] This purple fluorescence is intrinsic to the material and is ascribed to surface bound PTSA groups. This attribution is further backed by the absorbance spectra (**Figure 3C**) which shows three electronic transitions at 371nm, 279nm and 238nm with resolved vibronic levels separated by an average of ~185meV (6.70 μm). At higher concentrations, a green fluorescence peak appears **Figure 3A** and **3D**. At 1g/L the green peak is centred at 506nm and excited most strongly by 402nm, at this concentration the purple fluorescence is still present (**Figure 3D**, **Figure S8**). Increasing the concentration to 10g/L a redshift is observed in both the emission and excitation peaks, with peak emission at 526nm and peak excitation at 408 nm. The green emissions possess a broader FWHM of ~60nm, this is expected from a non-rigid structure with greater degrees of freedom.[24]

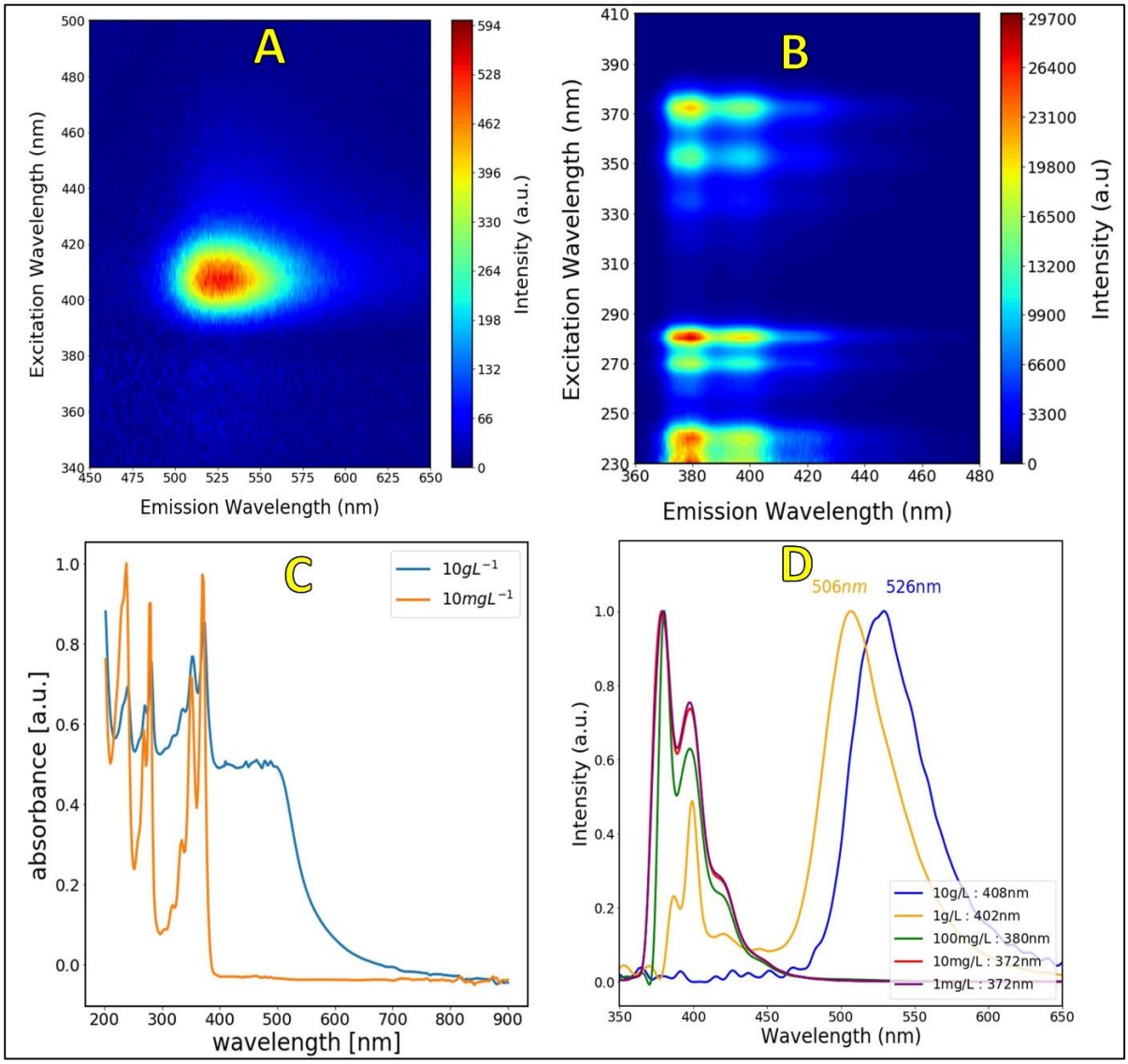

Figure 3: A: PL excitation-emission matrix for DCQDs; 10g/L. B: PL excitation-emission matrix for DCQDs; 10mg/L. C: Absorption spectra for DCQDs at 10g/L and 10mg/L. D: Concentration dependent PL emission spectra for DCQDs.

Due to the concentration dependence, spectral broadening, and the apparent lack of fluorophores other than PTSA, this fluorescence has been attributed to the formation of excimers between the surface bound PTSA groups. A quite similar excimer formation is observed in pyrene, the base molecule of PTSA, a feature which is utilised in fluorescence-based sensors capable of characterising the conformation and dynamics of proteins and polypeptides.[25] In the absorption spectra of higher concentrations (1g/L-10g/L) a visible

absorption peak can be seen beginning at 400nm and trailing off into the NIR range (**Figure 3C, S8**). This is the source of the gold-orange colour of the DCQDs solution, which is not present in PTSA. It is not certain if this is a consequence of the *sp2* hybridized core, inclusions of reaction intermediates, or additional absorption states due to the PTSA excimers. The full set of concentration dependent fluorescence and absorption spectra may be found in the supporting information (**S7 & S8**).

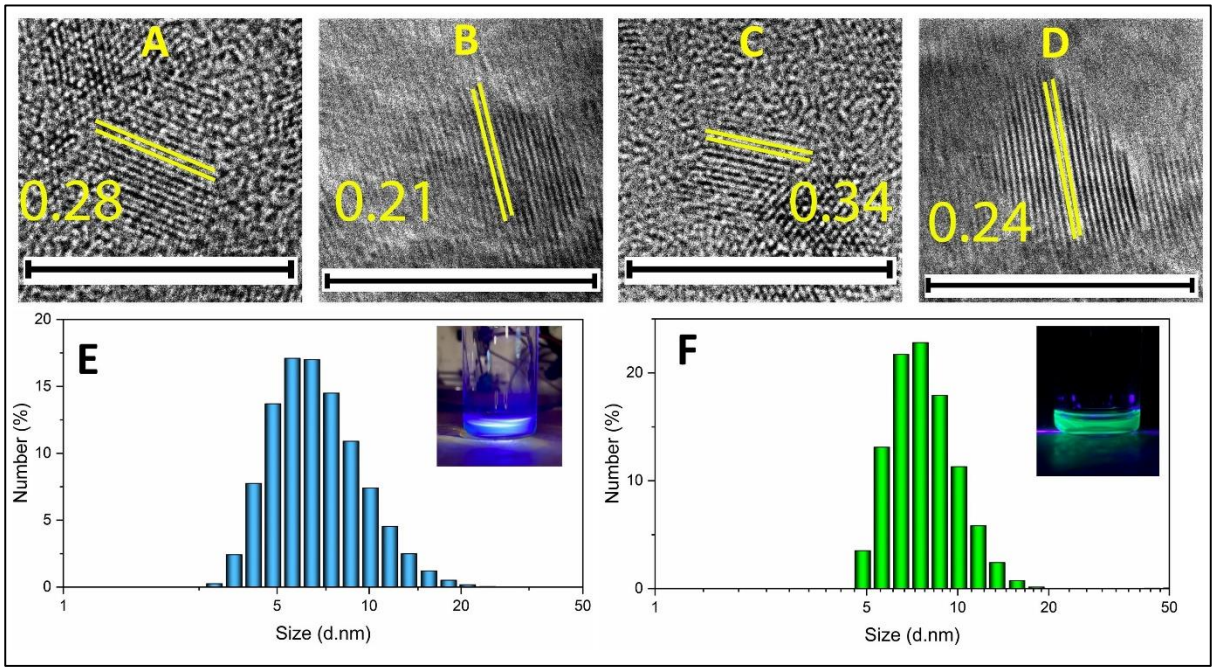

Figure 4: Microstructural and morphological features of the CQDs. A, B, C, D: HRTEM indicating lattice planes of CQDs (The scale bar is 10 nm), E: DLS size distributions of BCQDs (Inset: fluorescence images of BCQDs under UV light) F: DLS size distributions of DCQDs (Inset: fluorescence images of DCQDs under UV light)

The morphology and size distribution of the CQDs were determined by TEM and DLS. **Figures S2** and **S3** show the TEM images of the produced highly crystalline CQDs are spherical in shape and uniformly dispersed from each other. HRTEM and DLS size distributions are shown in **Figure 4**. The average size of BCQDs and DCQDs are to be 2.74 ± 1.01 and 2.40 ± 0.98 nm, respectively. DLS data revealed the mean hydrodynamic diameters of BCQDs and DCQDs are 5.61 and 7.53 nm, respectively. HRTEM data shows lattice fringes with spacings of 0.34 nm, 0.24 nm, 0.28 nm, and 0.21 nm which are attributed to (002)[26], (1120)[27], (002) and (100)

[28] planes. Considering the size distribution displayed on the corresponding histograms it can be concluded that the PL emission is not attributable to the quantum confinement effect. The emission properties of the synthesized BCQDs and DCQDs can be attributed to the surface states of the functional groups.[7, 26, 29]

Elemental composition analysis and surface states were determined by FT-IR and XPS. In the FTIR spectra (**Figure S4**) DCQDs showed a broad absorption from ~2500 to 3600 cm^{-1}, indicating the stretching vibrations of methylene (C-H), amino (N-H), and hydroxyl (O-H).[30] N doping can be identified by the C-NH bending vibration at 1416 cm^{-1} and N-H bending vibration at 1570 cm^{-1}. Other than the broad O-H stretching observed in 3300 – 2500 cm^{-1}, C-O stretching vibrations can be seen in 1635, 1124, 1050 and 994 cm^{-1}. These can also be attributed to the presence of carbonyl groups on the GCQDs. Further, C-H bending vibrations can be identified at 675 and 835 cm^{-1} which can be related to the deformed benzene rings by non-graphitic N doping.[13] The presence of hydroxyl and carboxyl groups are important for the water solubility of the synthesized CQDs.[31]

The X-ray photoelectron spectroscopy (XPS) results indicate the 21.7 % nitrogen composition in BCQDs. This is higher than most of the reported N-doped CQDs and is comparable with the results published by Lin et al.[30] N doping is highly desirable on number of CQD applications because it increases the fermi level, improves quantum yield and increase the analytical detection and reduction of electron hole recombination.[22] Nitrogen atomic composition of DCQDs is only 1.55 %, indicating air plasma can also dope nitrogen in trace amounts in absence of chemical nitrogen dopant. Similar nitrogen content of 1.21% has been reported in a previous study where microwave method was used under open atmosphere for the CQDs synthesis.[32] As shown in **Figure 5**, the high resolution XPS spectrum of C 1s can be deconvoluted into four peaks at 284.6, 286.0, 287.7, and 289.1 eV, which were attributed to

C=C/C-C, C-N/C-O/C-S, C≡N, and COOH, respectively. The XPS of N 1s spectra contained three components for N-H (401.6 eV), C=N-C (398.8 eV) and C-N-C (399.6 eV). The O 1s spectra was composed of two peaks at 531.8 and 533.0 eV for C=O and C-O.[30] FT-IR and XPS confirms that the surface of the CQDs contain hydroxyl and carbonyl groups. Also, N containing groups have been formed in DCQDs and doped into the structure. Additionally, the S 2p spectrum (**Figure S6**) of DCQD has two peaks. The peaks at 163.9 and 165.0 eV correspond to S $2p^{3/2}$ and S $2P^{1/2}$ spectra, respectively. This confirms the S containing PTSA groups coexist on the DCQD surface which cause the dual-emissive behaviour of the DCQDs.

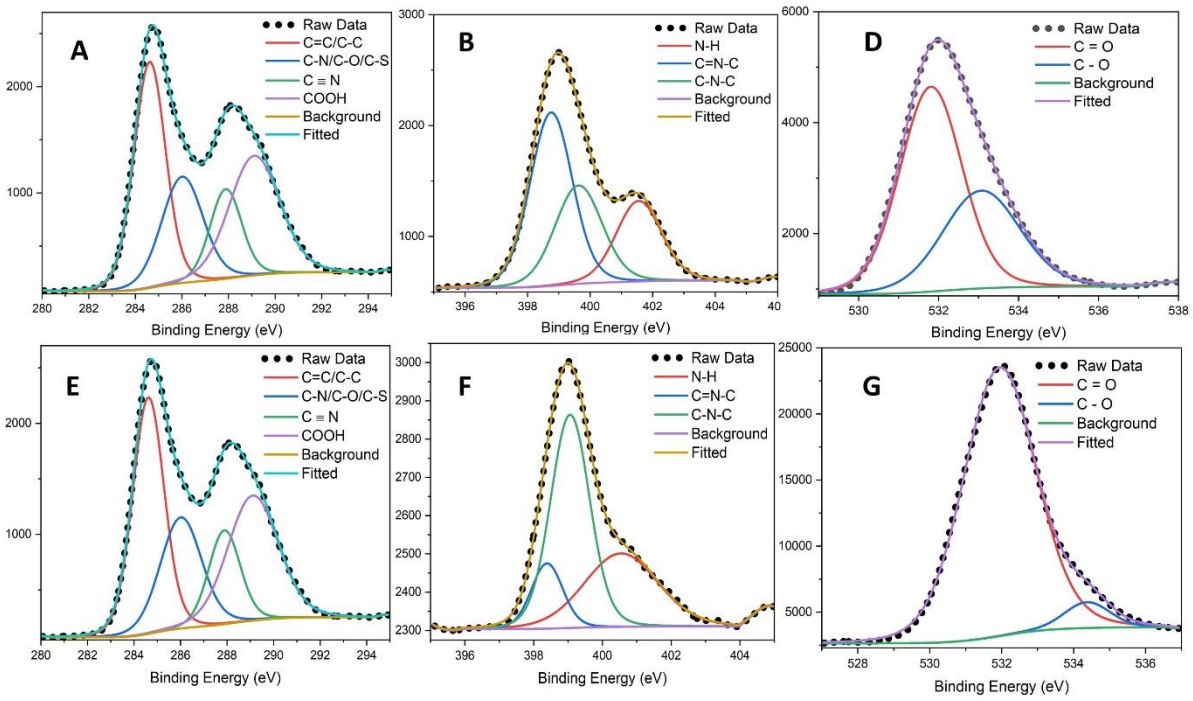

Figure 5: BCQD core level spectra, A: C1s, B: N1s, C: O1s, and DCQDs core level spectra, E: C1s, F: N1s, G: O1s

The synthetic approach for the preparation of the CQDs via cold atmospheric pressure plasma method is shown in **Figure 1**. Thermal images of the plasma plume were captured using an infrared camera with a thermal sensitivity of 0.07 ^{0}C (FLIR, Inc., FLIR ONE Pro) indicate the temperature is very close to the room temperature (**Figure S5** and supplementary video). It was observed that the temperature increased in the reaction medium up to 64°C during the

experiment. To investigate the influence of reaction temperature on the medium, a control test was conducted by heating precursor solution under similar condition in absence of cold plasma and neither colour change on the precursor medium nor CQD formation was detected.

Optical emission spectra (**Figure 6**) were recorded to identify the excited species generated inside the plasma which help to analyse the reaction mechanism. The second positive band system of N_2 can be seen in BCQD spectra corresponding to the C-B electronic transition. H_β transition at 656 nm and atomic oxygen at 777 nm[13] can be seen in both BCQD and DCQD spectra. High intensity sodium peaks at 588.9 and 589.6 nm[33] can be observed in DCQD spectra which inhibits most of the features of other lines. $C_4H_2^+(A^2\Pi - X^2\Pi)$[34] radical can be seen in BCQD OES spectrum and a faint signature can also be seen in the DCQD OES too. The relatively weak signature might be caused due to the high intensity of Na lines appearing in the spectrum and the presence of CN (B-X) violet system between 400-425 nm.[35] High intensity nitrogen species signatures can be seen in the BCQD OES and with significantly lower intensity in DCQD OES, which further support the nitrogen doping estimated in XPS results with 21.7% for BCQDs and 1.55% for DCQDs.

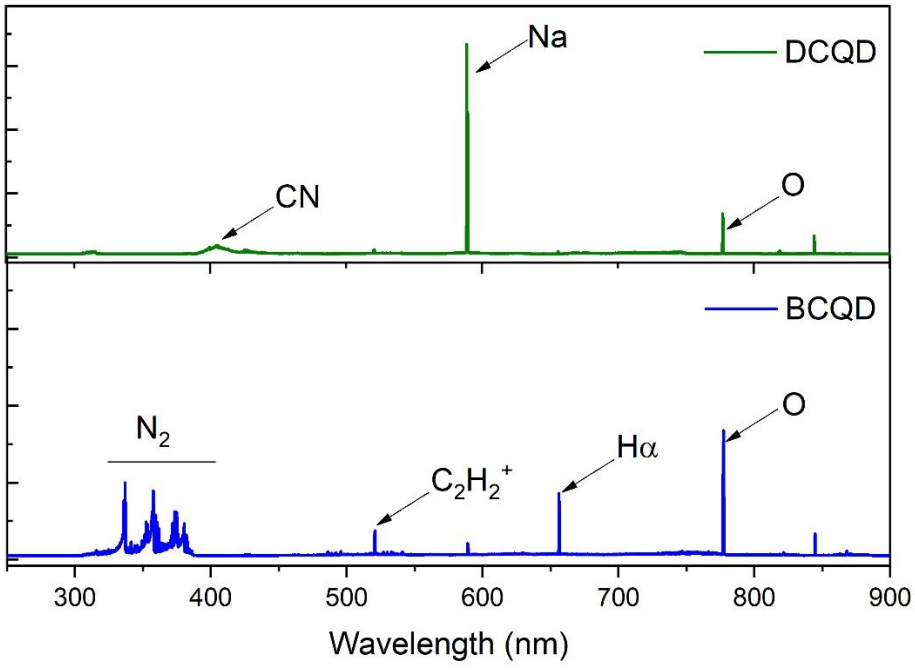

Figure 6: Optical emission spectra (OES) during the plasma treatment for DCQD and BCQD synthesis.

The precursor molecules transform through several stages during the synthesis of CQDs. The first stage is called condensation which makes chain intermediates. These intermediates are then polymerized and aggregated. Thirdly, carbonization or aromatization occurrs, and the last phase is further modification of the surface by various functional groups which also known as passivation. At the plasma-liquid interface, a number of complex electrochemical reactions occur. These may excite, ionize, or dissociate water and precursor compounds into molecular fragments such as OH, CH, C_2, $C_2H_2^+$, and H. O, H and OH radical production in the gas phase suggests the possibility to form other radicals such as H_3O^+. Solvated electrons (e_{aq}^-) are a very important constituent of the plasma liquid electrochemistry which participate to form OH radicals.[13] To identify the possible contribution of the e_{aq}^- for the CQDs synthesis, a control test was carried out which was adopted from work by Yang et al.[12] The results obtained were similar to their study, with a significant reduction in the formation of CQDs with the addition of Hydrogen peroxide (H_2O_2) in the precursor solution, which acts as an e_{aq}^- scavenger. Peaks in $C_2H_2^+$ radicals are observed during both BCQDs and DCQDs synthesis originating from the dissociation of the organic precursor. Xu et al. suggested that C_2 species are able to create super saturated partial pressure C to initiate nucleation of solid carbon clusters supported by CH radicals.[10] A similar process here may be dominated by $C_2H_2^+$ and nucleated carbon clusters in the gas phase which then transfer back to the liquid medium via the air flow. Surface functionalization of the formed CQDs take place in the liquid medium by reacting with the species in the solution. In the case of DCQDs formation, it is likely that the aromatic rings are opened due to the plasma irradiation [36], and the PTSA radicals combine and form the graphitic carbon cores.

Few reports can be found in the literature regarding dual-emissive CQDs synthesis with the emission colour combinations of blue-red[37], blue-green[38], green-red[39], red-yellow[40], red-orange[41], and blue-yellow.[42] Each of these studies has been conducted via thermal synthetic routes such as hydrothermal, solvothermal or microwave techniques which require temperatures above 85^0C within the reaction medium. Longer preparation times were also necessary and varied from hours to days in hydrothermal and solvothermal methods. However, the atmospheric pressure air plasma method presented here can produce DCQDs within the reaction time of a few minutes below 65^0C. The reduction of processing temperature and time is a significant advantage for the bulk synthesis of CQDs on a commercial scale. Also, this work opens the possibility to use thermal sensitive chemicals for further modifications/ enhancements of the CQDs in future works.

To seek further proof for the excimeric origin of the green emissions, time correlated single photon counting (TCSPC) was performed (Horiba delta time, Horiba Inc. Japan) on samples at concentrations of 10 g/L, 1 g/L and 10 mg/L; concentrations which show only green, green, and purple, and only purple emissions, respectively. Two excitation frequencies were used; 365 nm to probe the purple emissions, and 453nm for the green the results were fitted using mono or bi-exponential fitting. The results show that there are fundamentally two decay times at ~3-6 ns and ~10-14 ns, both of which are present at 453 nm excitation, and only the longer one is present at 365 nm (**Table 1, Figure 7A**). The short lifetime is attributed to the excimer, and the longer to the monomeric emission. These results are consistent with those published by J. B. Birks *et al*.[43] In their comprehensive study of excimer lifetimes in pyrene, however both excimer and monomer decay lifetimes in DCQDs are shorter than in pyrene. Similar to their results, a decrease in τ_2 is observed here with the increased concentration.

Concentration	Excitation	τ_1 (Percentage)	τ_2 (Percentage)	$\tau_{average}$
10g/L	453nm	$11.52 \pm 0.198\ ns$ (86.5%)	$3.85 \pm 0.227\ ns$ (13.5%)	$9.09 \pm 0.320\ ns$
1g/L	453nm	$13.35 \pm 0.212\ ns$ (87.4%)	$5.50 \pm 1.038\ ns$ (12.6%)	$11.32 \pm 1.059\ ns$
1g/L	365nm	$13.62 \pm 2.318\ ns$		$13.62 \pm 2.318\ ns$
10mg/L	365nm	$10.55 \pm 4.595\ ns$		$10.55 \pm 4.595\ ns$

Table 1: TCSPC results giving the fluorescent lifetimes for various concentrations of DCQDs

The potential for DCQs to act as fluorescent ion sensors was also investigated. The study was conducted by testing chemicals with common metallic cations at 50 ppm in a 10 mg/L solution of DCQDs, see **(Figure S10)** for the complement of cation sensitivities. It was found that they possess a strongly selective response to Cu^{2+} ions, in which the monomeric purple fluorescence is quenched, and the dimeric green signal is enhanced **(Figure 7B**). Whilst some other cations (Co^{2+}, Fe^{3+}, Ag^{1+} and K^{1+}) induce a moderate quenching of the purple monomeric fluorescence, the magnitude of quenching is much greater for Cu^{2+}, and only Cu^{2+} causes an enhancement of the excimer signal. Interestingly, this effect is only present after exposure to light capable of exciting the monomeric fluorescence. Light with the wavelengths greater than 400 nm did not induce a colour change. However, after the initial photoactivation with UV the change in emission is permanent. For concentrations of Cu^{2+} > 0.9 ppm the change in colour under UV is visible to the naked eye **(Figure 7D**) which is even lower than the WHO guideline for natural waters (2 ppm). This implies that with a simple UV light source DCQDs could be used to rapidly test water for safe levels of copper. The colorimetric changes were found to be insensitive to a reduction in concentration of the DCQDs to 1mg/L. It is suspected that this behaviour will hold for most concentrations below ~1 to 0.1g/L when concentration dependent excimer formation begins to manifest.

The quenching trend is semi-linear, showing a gentle positive curvature in the Stern-Volmer plot (**Figure 7C**). This may suggest a combination of complexation and collisional quenching. The enhancement effect on the other hand is more non-linear and shows signs of saturation toward the upper limit of testing. The difference is especially clear when plotting the fluorescence intensities of the two emission peaks against concentration (**Figure 7E**).

Due to the earlier study of concentration dependence, and the excitation-dependent feature of the Cu^{2+} sensing, it is proposed that the Cu^{2+} ions bind together with PTSA excimers after they form from the combination of a pair of surface-bound PTSA groups, at least one of which must be in an excited state. Once a bound excimer Cu^{2+} complex has been formed, it seems to be permanent, with chelating agent EDTA incapable of reversing the change in emissions. This may lead to a peripheral application as a highly selective and effective platform for the removal of copper.

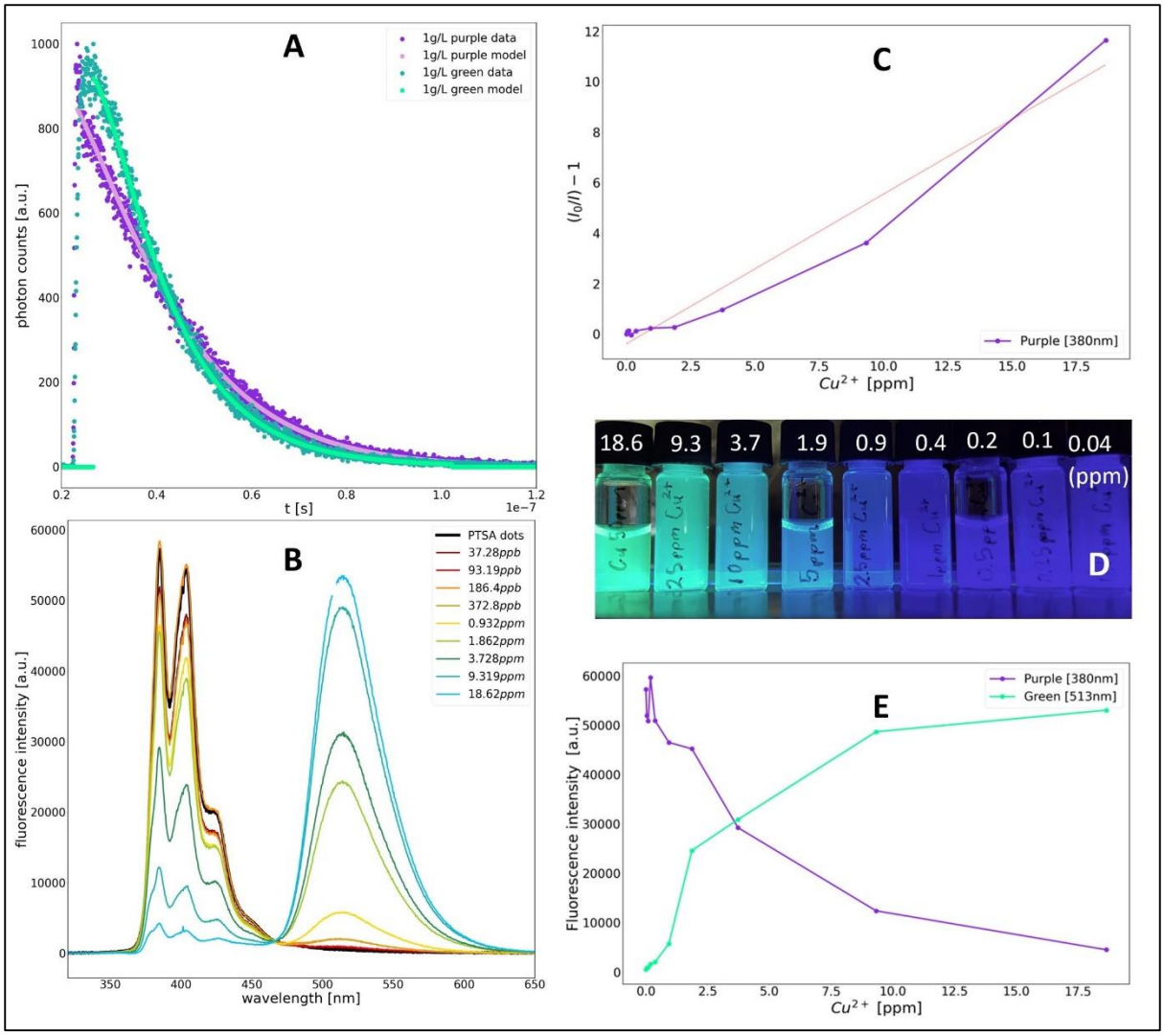

Figure 7: A: TCSPC decay results for DCQDs 1g/L @ 365nm and 453nm excitation. B: Cu^{2+} sensitivity of DCQD Fluorescence spectra. C: Stern-Volmer plot for the quenching of purple fluorescence signal. D: Photograph of DCQDs with Cu^{2+} ions at various concentrations. E: Concentration dependence of purple and green peaks in response to Cu^{2+}.

Conclusion

Atmospheric pressure air plasma has been used to synthesize green and blue dual emissive CQDs under ambient conditions. Two synthesis systems were demonstrated, the first one carbonizes citric acid and simultaneously incorporates N through addition of urea, and the second system involves combining the aromatic rings of pyrene tetrasulfonic acid. The DCQDs maintained the emission features of PTSA despite the formation of CQDs. The emission

wavelengths are about 380-400 nm in low concentration and 515 nm in high concentration. Solvated electrons generated during the air plasma treatment play a major role in the CQDs formation. Compared to the previous works in literature the synthetic time was reduced significantly. This synthesis method can be carried out in ambient conditions without complex equipment. DCQDs and BCQDs can be produced in scalable manner, helpful for their potential applications. To explore the possible applications of the DCQDs, their use in fluorescent ion sensor to detect Cu^{2+} was demonstrated as a proof-of-principle. This study provides fundamental knowledge on air plasma assisted CQDs synthesis with a potentially scalable option for the mass production.

3. Experimental

4.1. Materials and methods

Schematic Diagram of the Preparation Procedure of CQDs is given in **Figure 1** and the experimental setup is shown in **Figure S1**. An atmospheric air plasma system (Nanjing Suman Plasma Technology® Model PG-1000 Z/E) was connected to an air pump unit (Nanjing Suman Plasma Technology® Model FP-290). The precursor solution for the synthesis of BCQDs is prepared by dissolving 5 g of citric acid (Sigma Aldrich®) and 10 g of urea (Univar®) in 100 mL of ultra-pure water. The precursor solution was placed 5 cm below the plasma nozzle. For the synthesis of DCQDs, 6 g of pyrenetetrasulfonic acid tetrasodium salt hydrate was dissolved in 100 mL of ultra-pure water to be use as the precursor solution. A continuous atmospheric air flow of 240 L/min was supplied throughout the experiment. The plasma treatment was conducted for 10 min and the solution was dialyzed with 1-3.5 k Da membrane to remove larger particles and unreacted precursors. The produced solution is dried and used for further characterisations. Dry weight of the purified DCQDs weighted 23.5 mg, making percentage yield of 0.39%.

4.2. Characterization

The optical emission spectrum (OES) was measured by using an Andor SR-500® spectrometer, Newton® CCD camera and fibre optic cable. Malvern Zetasizer Nano ZS® was used for the Dynamic Light Scattering (DLS) measurements to determine the size distribution. The UV-Vis spectra were recorded on a UV-Vis spectrometer (Cary 60 UV-Vis Spectrophotometer, Agilent Technologies®, USA). The detailed absorbance and fluorescence spectra and QY of DCQDs were recorded on a HORIBA Duetta spectrofluorometer, Horiba Inc. Japan. The quantum yield measurements were performed with quinine sulfate in 0.5M sulfuric acid as a reference. The transmission electron microscopy (TEM) measurements were performed by JEOL 2100® TEM. During the sample preparation, carbon dots suspended aqueous solution was added dropwise on lacy carbon coated copper TEM grids and dried under an IR lamp for 10 minutes. X-ray photoelectron spectrometer (XPS) analysis was carried out by Kratos AXIS Supra® photoelectron spectrometer. Fourier-transform infrared (FT-IR) spectra were taken down in a Bruker® ATR instrument from 400 -4000 cm $^{-1}$ with a resolution of 4 cm^{-1}. Photoluminescence spectra of excitation and emission of both CDs were recorded on Fluorescence Spectrophotometer Eclipse G9800A (Cary®).

Supporting Information

Supporting Information is available from the Wiley Online Library or from the author.

Acknowledgements

The work was partially supported by the Australian Research Council (ARC). The authors would like to acknowledge the support given by QUT HDR tuition fee scholarship. QUT–Central Analytical Research Facility (CARF) for technical support and characterization.

Author contributions

Janith Weerasinghe and James Scott have made equal contributions. Janith Weerasinghe: Conceptualization, Methodology, Validation, Investigation, Writing - original draft, James Scott: Writing – original draft, Methodology, Validation, Formal analysis. Kasub Deshan: Formal analysis, Investigation. Dechao Chen: Methodology, Validation, Formal analysis. Amandeep Singh: Validation, Resources. Suvankar Sen: Formal analysis, Investigation, writing. Qin Li: Validation, Methodology, Resources, Supervision, review & editing. Prashant Sonar: Validation, Resources, Supervision. Krasimir Vasilev: Resources, Writing - review & editing, Supervision. Kostya (Ken) Ostrikov: Conceptualization, Methodology, Validation, Resources, Writing - review & editing, Supervision.

Conflict of interest

The authors declare no conflict of interest.

Received: ((will be filled in by the editorial staff))
Revised: ((will be filled in by the editorial staff))
Published online: ((will be filled in by the editorial staff))

References

[1] P. Yang, Z. Zhu, T. Zhang, M. Chen, Y. Cao, W. Zhang, X. Wang, X. Zhou, W. Chen, Carbon 2019, 146, 636.

[2] N. Tejwan, S. K. Saha, J. Das, Advances in colloid and interface science 2020, 275, 102046.

[3] J. R. Bhamore, S. Jha, T. J. Park, S. K. Kailasa, Journal of Photochemistry and Photobiology B: Biology 2019, 191, 150.

[4] F. Yan, Z. Sun, H. Zhang, X. Sun, Y. Jiang, Z. Bai, Microchimica Acta 2019, 186, 1.

[5] S. Wu, W. Li, Y. Sun, X. Zhang, J. Zhuang, H. Hu, B. Lei, C. Hu, Y. Liu, Journal of colloid and interface science 2019, 555, 607.

[6] H.-F. Xiong, B.-L. An, J.-M. Zhang, C.-l. Yin, X.-H. Wang, J.-H. Wang, J.-Q. Xu, Materials Today Communications 2020, 101762.

[7] X. Wang, Y. Feng, P. Dong, J. Huang, Frontiers in chemistry 2019, 7, 671.

[8] W. Song, W. Duan, Y. Liu, Z. Ye, Y. Chen, H. Chen, S. Qi, J. Wu, D. Liu, L. Xiao, C. Ren, X. Chen, Analytical Chemistry 2017, 89, 13626.

[9] W. H. Chiang, D. Mariotti, R. M. Sankaran, J. G. Eden, K. Ostrikov, Advanced Materials 2020, 32, 1905508.

[10] H. Xu, C. He, L. Lin, J. Shen, S. Shang, Materials Letters 2019, 255, 126532.

[11] M. K. Thakur, C.-Y. Fang, Y.-T. Yang, T. A. Effendi, P. K. Roy, R.-S. Chen, K. K. Ostrikov, W.-H. Chiang, S. Chattopadhyay, ACS Applied Materials & Interfaces 2020, 12, 28550.

[12] J.-S. Yang, D. Z. Pai, W.-H. Chiang, Carbon 2019, 153, 315.

[13] D. Kurniawan, W.-H. Chiang, Carbon 2020, 167, 675.

[14] J. Amaro-Gahete, M. Mora, P. Gutiérrez, D. Cosano, D. Esquivel, J. R. Ruiz, C. Jiménez-Sanchidrián, M. C. García, F. J. Romero-Salguero, Journal of Physics D: Applied Physics 2020, 53, 435202.

[15] Z. Wang, Y. Lu, H. Yuan, Z. Ren, C. Xu, J. Chen, Nanoscale 2015, 7, 20743.

[16] X. Huang, Y. Li, X. Zhong, A. E. Rider, K. Ostrikov, Plasma Processes and Polymers 2015, 12, 59.

[17] Q. Wang, Q. Zhang, Y. Chen, J. He, K. Jiang, Z. Hu, X. Zhong, Plasma Processes and Polymers 2018, 15, 1700088.

[18] X. Ma, S. Li, V. Hessel, L. Lin, S. Meskers, F. Gallucci, Chemical Engineering and Processing-Process Intensification 2019, 140, 29.

[19] X. Ma, S. Li, V. Hessel, L. Lin, S. Meskers, F. Gallucci, Chemical Engineering Science 2020, 220, 115648.

[20] A. Dager, A. Baliyan, S. Kurosu, T. Maekawa, M. Tachibana, Scientific reports 2020, 10, 1.

[21] X. Qin, J. Liu, Q. Zhang, W. Chen, X. Zhong, J. He, Nanoscale research letters 2021, 16, 1.

[22] Y. Liu, S. Luo, P. Wu, C. Ma, X. Wu, M. Xu, W. Li, S. Liu, Analytica chimica acta 2019, 1090, 133.

[23] L. Allamandola, A. Tielens, J. Barker, The Astrophysical Journal Supplement Series 1989, 71, 733; E. Bakes, A. Tielens, C. W. Bauschlicher Jr, D. M. Hudgins, L. J. Allamandola, The Astrophysical Journal 2001, 560, 261.

[24] N. Nijegorodov, W. Downey, The Journal of Physical Chemistry 1994, 98, 5639.

[25] R. Casier, J. Duhamel, Macromolecules 2018, 51, 3450; G. Bains, A. B. Patel, V. Narayanaswami, Molecules 2011, 16, 7909.

[26] C. Reckmeier, J. Schneider, A. Susha, A. Rogach, Optics express 2016, 24, A312.

[27] T. Orriere, D. Kurniawan, Y.-C. Chang, D. Z. Pai, W.-H. Chiang, Nanotechnology 2020, 31, 485001.

[28] R. Atchudan, T. N. J. I. Edison, K. R. Aseer, S. Perumal, N. Karthik, Y. R. Lee, Biosensors and Bioelectronics 2018, 99, 303.

[29] F. Yan, Y. Jiang, X. Sun, Z. Bai, Y. Zhang, X. Zhou, Microchimica Acta 2018, 185, 1.

[30] C. Lin, Y. Zhuang, W. Li, T.-L. Zhou, R.-J. Xie, Nanoscale 2019, 11, 6584.

[31] D. B. Gunjal, Y. M. Gurav, A. H. Gore, V. M. Naik, R. D. Waghmare, C. S. Patil, D. Sohn, P. V. Anbhule, R. V. Shejwal, G. B. Kolekar, Optical Materials 2019, 98, 109484.

[32] A. Singh, E. Eftekhari, J. Scott, J. Kaur, S. Yambem, F. Leusch, R. Wellings, T. Gould, K. Ostrikov, P. Sonar, Sustainable Materials and Technologies 2020, 25, e00159.
[33] A. Kramida, Y. Ralchenko, J. Reader, N. A. Team, 2020.
[34] F. Guzmán, M. Ruiz, E. Valderrama, M. Favre, H. Bhuyan, E. Wynham, H. Chuaqui, "Spectroscopic characterization of RF hydrocarbon plasmas for DLC coatings", presented at *Journal of Physics: Conference Series*, 2014.
[35] E. Carbone, F. D'Isa, A. Hecimovic, U. Fantz, Plasma Sources Science and Technology 2020, 29, 055003.
[36] R. Zhou, R. Zhou, J. Zhuang, Z. Zong, X. Zhang, D. Liu, K. Bazaka, K. Ostrikov, PloS one 2016, 11, e0155584; Z. Zhang, X. Gong, S. Zhang, H. Yang, Y. Shi, C. Yang, X. Zhang, X. Xiong, X. Fang, Z. Ouyang, Scientific reports 2013, 3, 1.
[37] W. Li, S. Wu, H. Zhang, X. Zhang, J. Zhuang, C. Hu, Y. Liu, B. Lei, L. Ma, X. Wang, Advanced Functional Materials 2018, 28, 1804004.
[38] S. Kainth, B. Maity, S. Basu, Materials Science and Engineering: C 2020, 108, 110443.
[39] M. Zhang, T. Zheng, B. Sheng, F. Wu, Q. Zhang, W. Wang, J. Shen, N. Zhou, Y. Sun, Chemical Engineering Journal 2019, 373, 1054.
[40] J. Liu, Y. Chen, L. Wang, M. Na, H. Chen, X. Chen, Journal of agricultural and food chemistry 2019, 67, 3826.
[41] M. Zhang, R. Su, J. Zhong, L. Fei, W. Cai, Q. Guan, W. Li, N. Li, Y. Chen, L. Cai, Nano Research 2019, 12, 815.
[42] F. He, J. Bai, Y. Cheng, K. Weerasinghe, X. Meng, H. Xu, W. Zhang, X. Fang, H.-B. Li, T. Ding, The Journal of Physical Chemistry C 2021, 125, 5207.
[43] J. Birks, D. Dyson, I. Munro, Proceedings of the Royal Society of London. Series A. Mathematical and Physical Sciences 1963, 275, 575.

Table of contents description and figure

A fast, effective, and single-step method is developed for the bulk synthesis of monochromatic blue and switchable blue-green carbon quantum dots (CQDs) by room-temperature air plasma processing, and the emission mechanisms are revealed. A proof-of-principle demonstration of fluorescence sensing of Cu^{2+} ions opens new opportunities for CQDs applications in environmental and biomedical sensing.

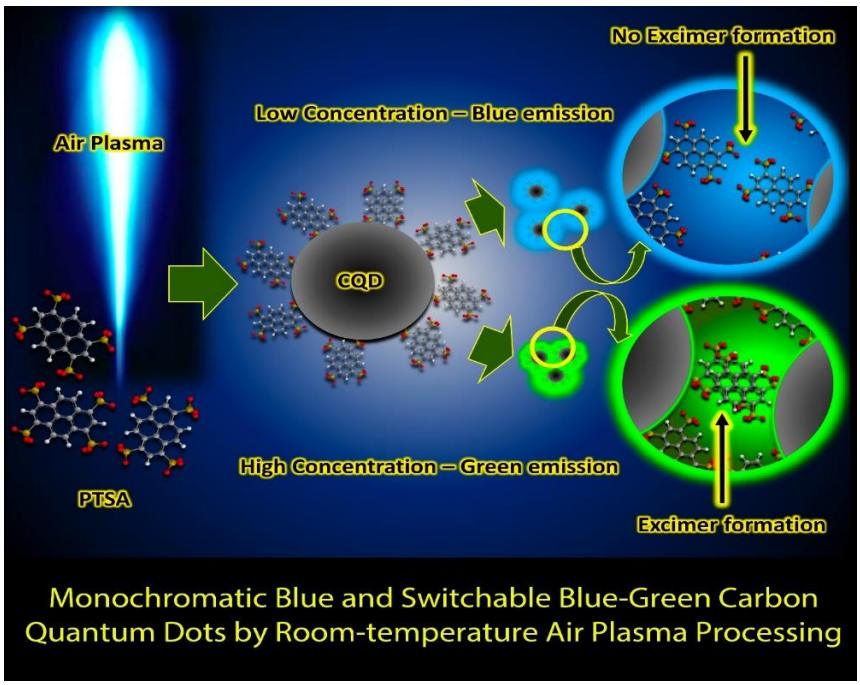

Supporting Information

Monochromatic Blue and Switchable Blue-Green Carbon Quantum Dots by Room-temperature Air Plasma Processing

Janith Weerasinghe, James Scott, Athukoralalage Don K. Deshan, Dechao Chen, Amandeep Singh, Suvankar Sen, Prashant Sonar, Krasimir Vasilev, Qin Li, and Kostya (Ken) Ostrikov**

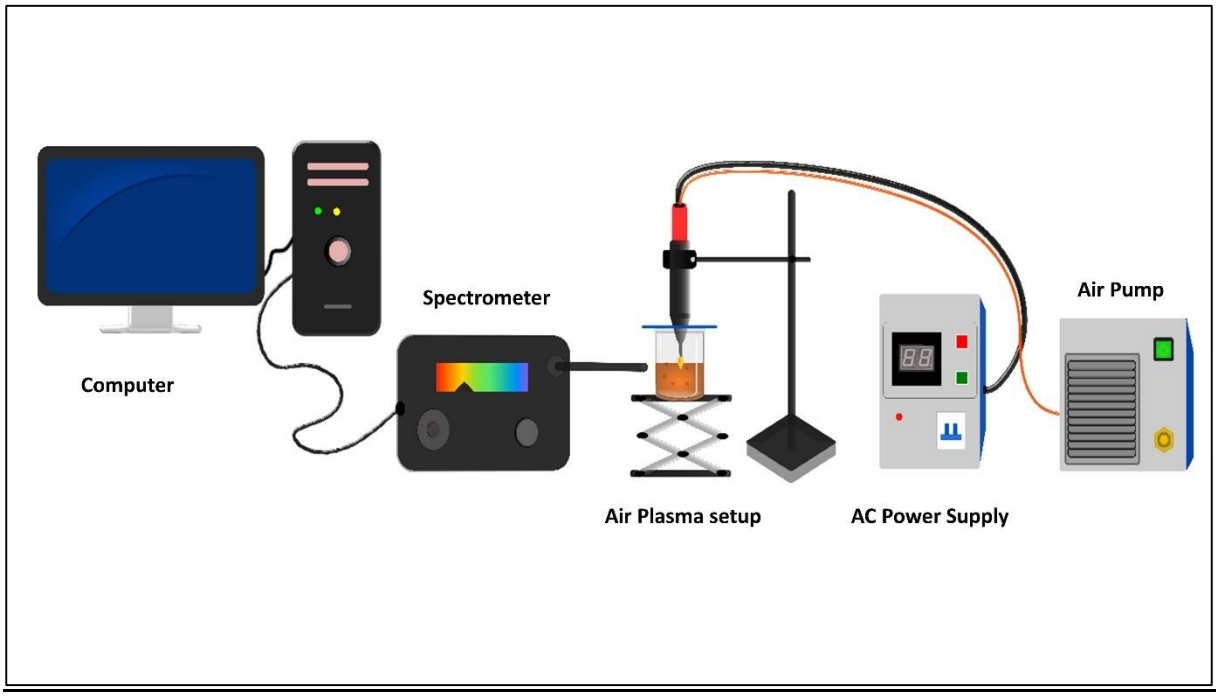

Figure S1: schematic diagram of the experimental setup used for the CQDs Preparation by air plasma technique

Figure S1 shows the experimental apparatus used for the CQDs preparation. The air pump filters the atmospheric air and feeds it to the air plasma nozzle which is ignited by the electric current from the AC power supply. The precursor solution kept in a beaker and subjected for the air plasma treatment. The optical emission spectrometer connected to the computer taking live readings from the plasma source for the identification of plasma species generated.

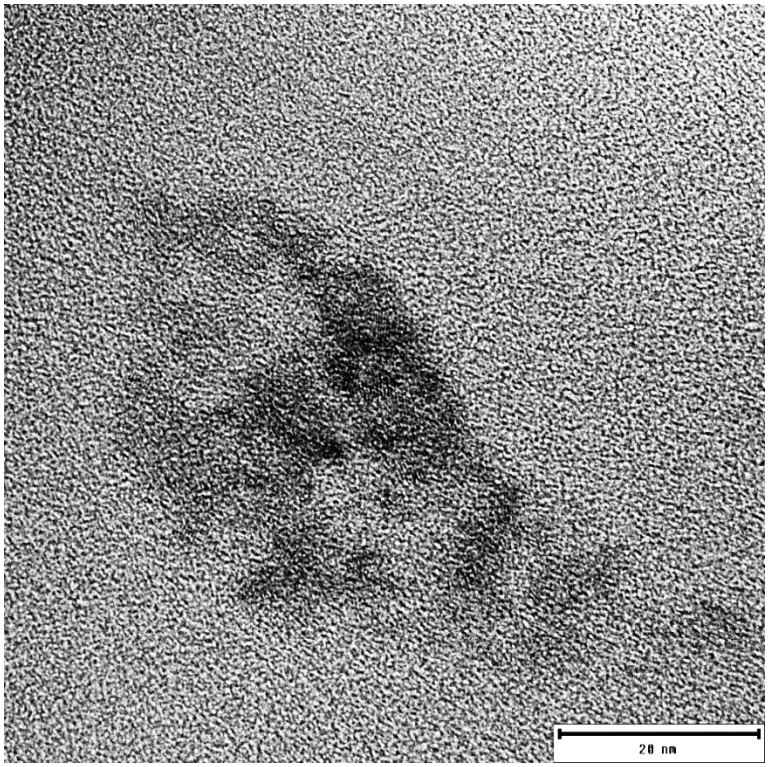

Figure S2: TEM image of a BCQD sample with lattice fringes

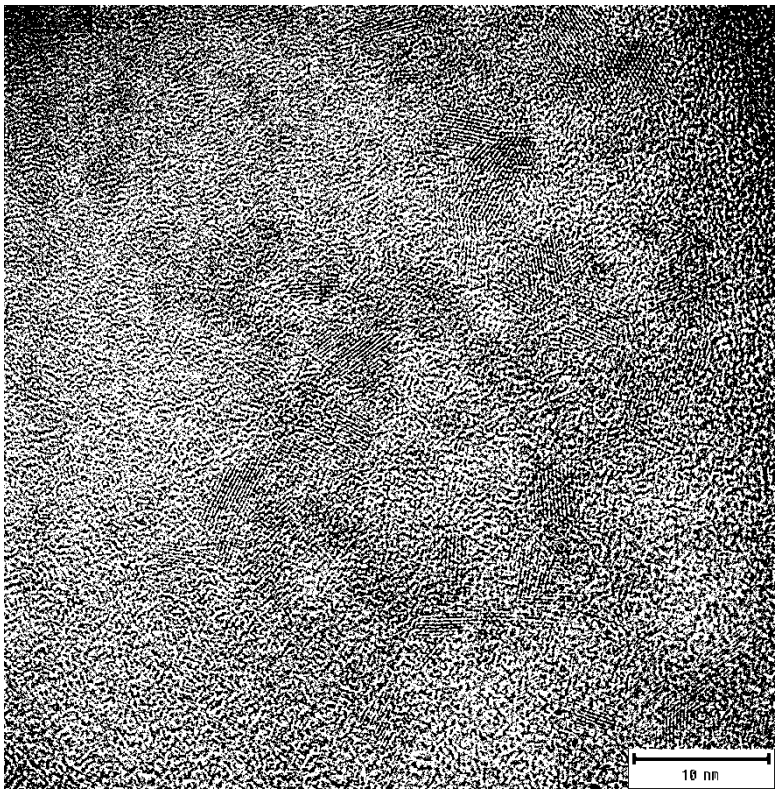

Figure S3: TEM image of DCQDs revealing lattice fringes

Figure S2 and S3 shows the TEM images of the BCQDs and DCQDs. Lattice planes of CQDs are also slightly visible where HRTEM images were taken to measure lattice distances.

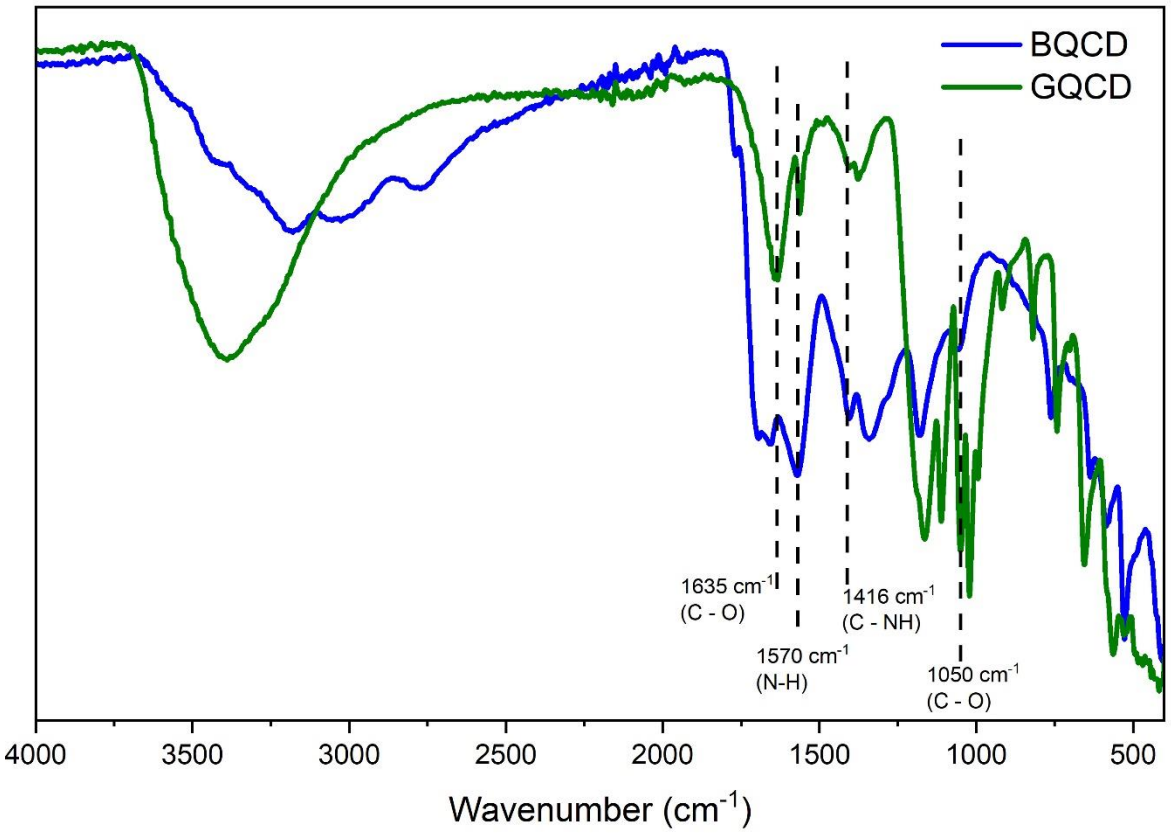

Figure S4: FTIR spectra of BCQDs and DCQDs. Significant increase of the nitrogen related peaks can be seen in BCQDs comparative to the DCQDs which confirms the N doping on the CQDs surface.

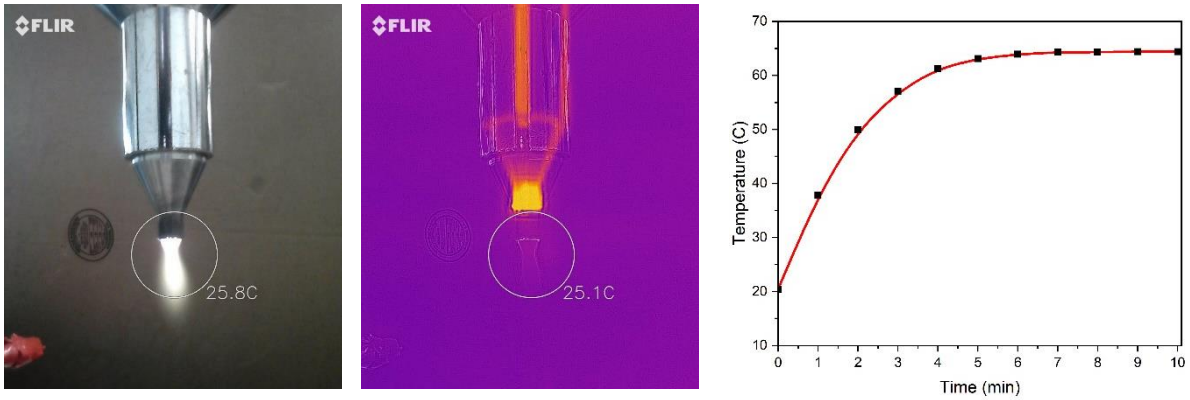

Figure S5: Left: visible and thermal images of the plasma jet measuring the infrared temperature while in operation. Right: Temperature variation of the sample with plasma treatment duration

Thermal camera imaging has been used to measure the temperature of the operating plasma as shown in **Figure S5.** Thermal imaging indicates the plasma temperature is very close to the room temperature.

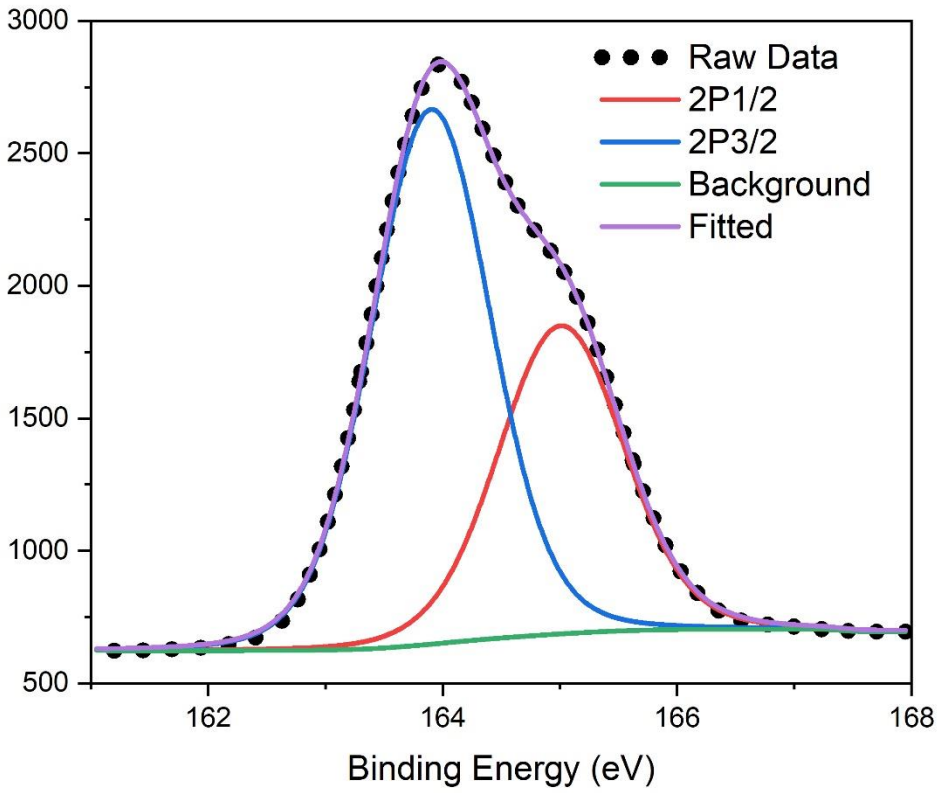

Figure S6: Component-fitted S2p signals on DCQDs

Component fitted XPS S2p signal is shown in **Figure S6** indicating the presence of sulphur containing groups on the surface on the DCQDs. This is an evidence for the surface pyrene groups which forms excimers on high DCQD concentrations which makes a longer wavelength shift in the emission spectrum.

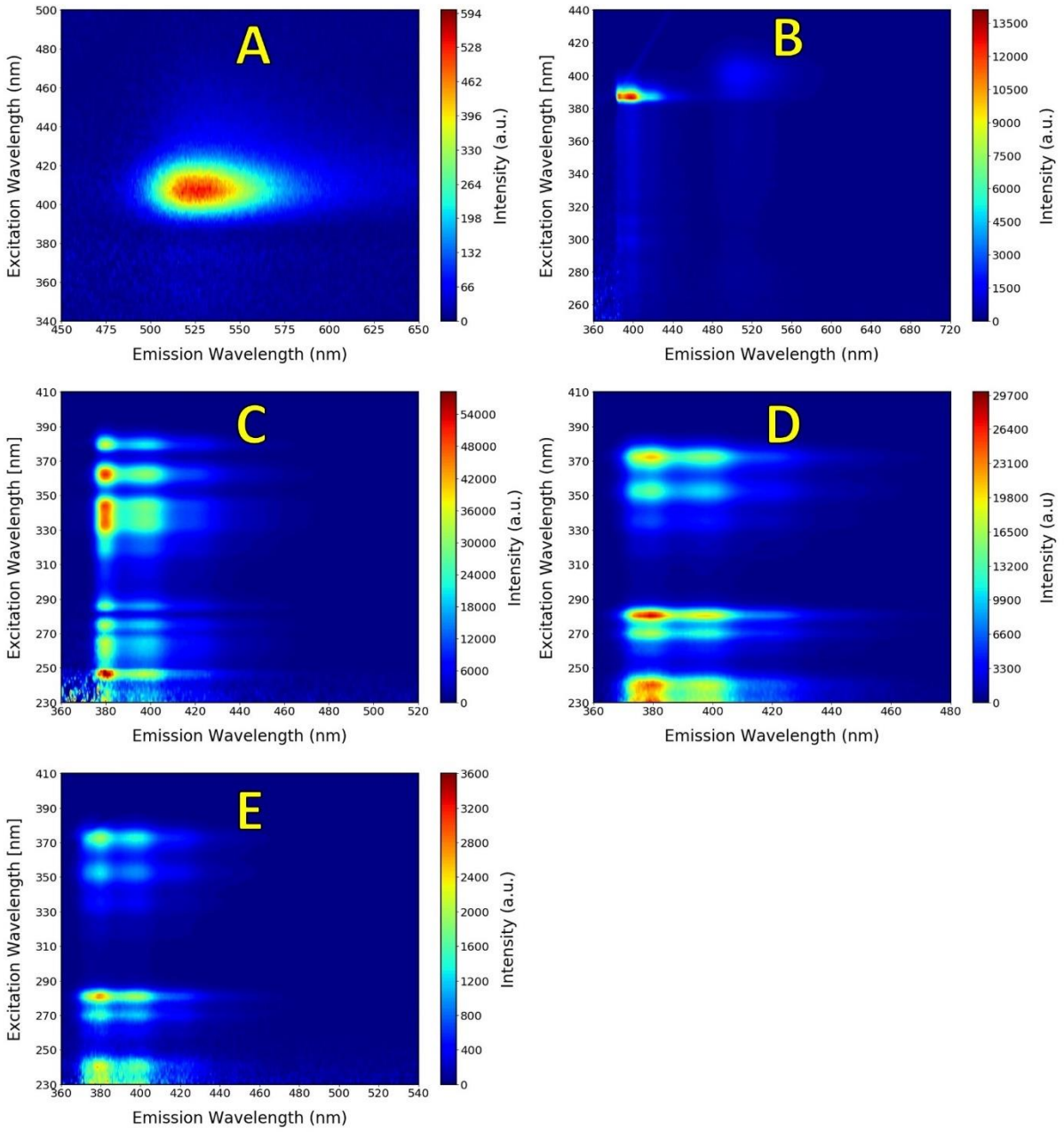

Figure S7: PL excitation-emission matrix for DCQDs A: 10g/L, B:1g/L, C: 100mg/L, D: 10mg/L, E: 1mg/L

Table T1: Excitation peaks and their associated excitation frequencies for DCQDs

Concentration	Emission Peaks (Excitation)
10g/L	526nm (408nm)
1g/L	506nm (402nm); 420nm, 398nm, 388nm (386nm)
100mg/L	421nm, 398nm, 380nm (380nm, 362nm, 344nm, 334nm, 286nm, 274nm, 264nm, 248nm, 230nm)
10mg/L	421nm , 398nm , 378nm (372nm, 352nm, 336nm, 280nm, 270nm, 234nm)
1mg/L	421nm , 398nm , 378nm (372nm, 352nm, 336nm, 280nm, 268nm, 230nm)

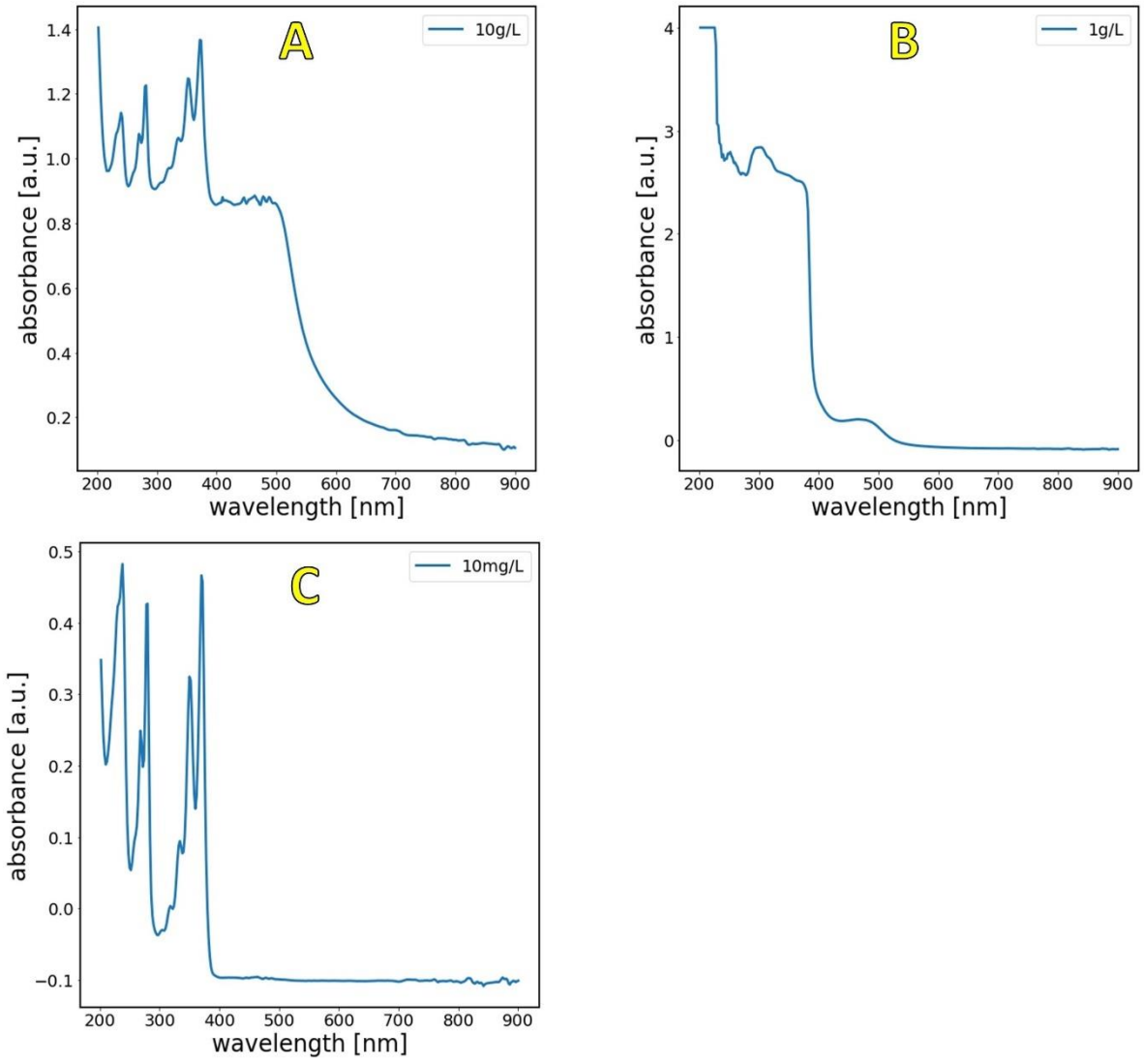

Figure S8: Absorption spectra for DCQDs A: 10g/L, B:1g/L, C: 10mg/L

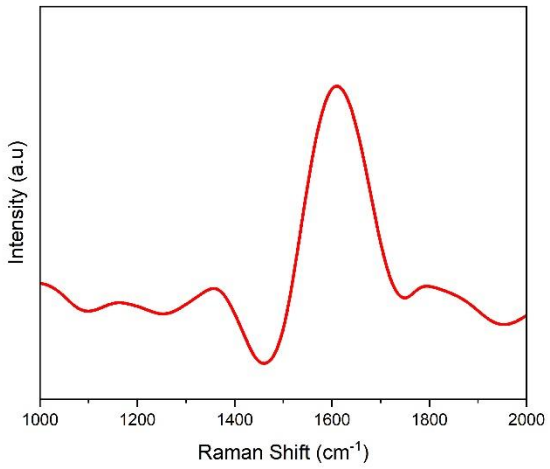

Figure S9: Raman spectra of the GCQDs indicating the graphitization of them

Raman spectrum was obtained by *inVia – Reinshaw* Raman spectrometer at 532 nm. Baseline corrected signal was FFT smoothed due to the high signal to noise ratio. G band and disordered D band signals at 1578 cm^{-1} and 1346 cm^{-1} were identified on the spectrum which indicates the graphitization of the CQDs.

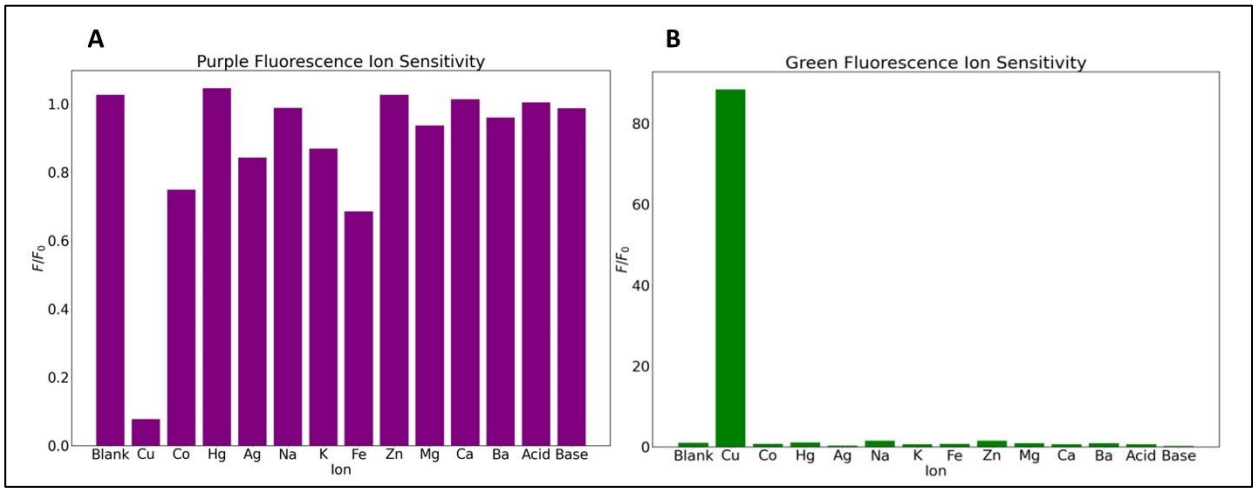

Figure S10: Ion sensitivity of both purple A: and green B: emissions of DCQDs. Initial sensitivity was tested at analyte concentrations of 50ppm by mass.